Tribology International 130 (2019) 366–377

Contents lists available at ScienceDirect

Tribology International

journal homepage: www.elsevier.com/locate/triboint

Transient aspects of plasma luminescence induced by triboelectrification of polymers

Debashis Puhan[a,*], Roman Nevshupa[b], Janet S.S. Wong[a], Tom Reddyhoff[a]

[a] Tribology Group, Department of Mechanical Engineering, Imperial College London, London, SW7 2AZ, UK
[b] Spanish National Research Council, "Eduardo Torroja" Institute (IETCC-CSIC), C/Serrano Galvache 4, Madrid, 28033, Spain

ARTICLE INFO

Keywords:
Triboelectrification
Luminescence
Charge
Plasma
Triboplasma
Discharge
Polymer
PTFE
UHMWPE

ABSTRACT

Transient electric gas discharges that occur around sliding interfaces during contact electrification of polymers were studied at millisecond timescales and with micrometre resolution. Deduced vibrational temperatures indicate cold plasma resulting from positive corona discharge. At millisecond timescales, previously unseen rapid discharge events are observed, and modelling suggests that these result from streamer development, triggered by electron emission from the polymer surface. Those which occur over a period of several seconds are shown to be caused by competition between charge generation and the formation of polymer films. The findings explain the interplay between charging and plasma generation and their dependence on wear processes.

1. Introduction

Tribocharging, or triboelectrification, is defined as the electrical charging of contacting insulators that occurs when they are rubbed together or brought in contact and then separated. The underlying physics of tribocharging is only now becoming understood [1], despite documents of its occurrence dating back thousands of years. Emergence of new technologies such as distributed energy harvesting by triboelectric nanogenerators [2] [3], nano-coulomb molecular mass spectrometry [4] and triboelectric X-ray source [5] as well as rapid development of the existing technologies, *e.g.* xerography [6], laser printing [7], electrostatic separations [8], and so on, have led to renewed interest in deepening our knowledge about the relevant phenomena of charge generation and dissipation [9]. Although the details of charging mechanisms are still incompletely understood, many efforts have been made on surface engineering of polytetrafluoroethylene (PTFE) and other polymer membranes to enhance the triboelectric output and to increase the surface charge density, which is closely approaching the maximum value that is constrained by air breakdown [9–11]. What has made this field challenging is that charging is not only an electrostatics problem, i.e. charge generation and dissipation, but in reality involves tribological processes, which are system dependent.

Early research led to the construction of a triboelectric series which ranks materials based on charge accumulation ([*e.g.* Refs. [12–14]]). However, the exact order of this series is inconsistent [15,16], and even rubbing together identical materials can produce charge [17,18] or de-electrification [19]. Furthermore, whereas for metals electron transfer between valence levels is understood to be the dominant mechanism [20], there has been uncertainty regarding charge transfer for insulating materials such as polymers, which by definition have no free charge carriers. Charge carriers in these contacts were initially assumed to be electrons [21–23] and then evidence suggested molecular or atomic ions [15,24–26], with the latter now being the more accepted view.

During the last decade, the picture of how both micro- and nanoscale events are responsible for tribocharging and inconsistencies in triboelectric series has become clearer, thanks in part to the introduction of Kelvin Probe Force Microscopy measurements [27]. Baytekin et al. showed that a mass transfer mechanism for tribocharging of polymers gives rise to nanoscale regions of positive and negative charge [28]. Following this, Galembeck and co-workers showed that polyethylene (PE) and PTFE, tribocharged due to the mechanochemical process of chain scission followed by electron transfer [29], with further support of mass transfer as a mechanism coming from Williams [30], Burgo and Erdemir [31].

An additional complication, which affects charging behaviour, is the role of the ambient environment [31] and humidity [32]. Furthermore, as shown by Sow et al., material strain can reverse the direction of

* Corresponding author.
E-mail address: d.puhan13@imperial.ac.uk (D. Puhan).

https://doi.org/10.1016/j.triboint.2018.09.026
Received 28 May 2018; Received in revised form 9 August 2018; Accepted 25 September 2018
Available online 06 October 2018

charge transfer [33] and may play a key role in triboelectrification in general. Despite these system-specific issues, several studies [31,34,35] suggest that tribocharging and friction force have a common origin and that measurements of the former provide fundamental information on the origins of the latter.

Discharging mechanisms have received considerably less attention and are not well understood [25]. Some evidence suggests that corona discharge limits the formation of charge during contact electrification [36–38]. When an electric field exceeds a threshold (30 kV/cm for air [39]), breakdown occurs that leads to the generation of plasma. The presence of this plasma was first predicted in 1965 [40], but it was not until the beginning of the XXI century that Nakayama and co-workers proved its existence by obtaining images of UV photon distributions in the vicinity of sliding contacts between a diamond tip and a dielectric surface [41–43]. It was found that the gas discharge at a sliding contact is not exactly the same as the gas discharges, which appear during the breaking of adhesive bonds, such as peeling a tape [44]. Besides controlling charge recombination, the generation of plasma is responsible for tribochemical behaviour that cannot be explained by classical means such as flash temperature rise [45,46]. For instance, plasma may induce reactions that alter contact conditions by forming breakdown products that deposit on component surfaces [47]. Plasma generated in this way can cause the degradation of polymeric components and organic lubricants, particularly in the case of computer hard drive applications [48]. It can also influence electric and mechanical properties of the materials of the sliding parts [49], that leads to complex nonlinear behaviour of energy and charge dissipation. At a larger scale, plasma generation at fault asperities, has been linked to seismo-electromagnetic radiation preceding earthquakes [50].

Despite the advances described above, there is still much uncertainty regarding triboplasma phenomena and its links with triboelectrification. Most critically, the vast majority of triboplasma measurements to date have been either time-averaged (*e.g.* Refs. [41,45,50–53]) or spatially averaged [25], and as a result, there is little understanding of the transient nature of this phenomenon. Furthermore, the focus of triboplasma and triboelectrification studies has been on crystalline inorganic materials, with only very few studies [25,54–57] addressing polymer materials, known to be important in tribocharging applications [9].

The aim of the current study is to elucidate the transient behaviour of tribocharging and its relationship to triboplasma for two polymers: ultra-high molecular weight polyethylene (UHMWPE) and polytetrafluoroethylene (PTFE). These two polymers are widely used as tribological materials in engineering and biomedical applications for their low wear (UHMWPE) and low friction (PTFE) properties. Furthermore, PTFE and PE have been studied extensively with respect contact electrification behaviour [29,58,59]. It is understood that, when rubbed, its dominant charging mechanism is the homolytic scission of the C—C bond which produces free radicals with markedly different electronegativities followed by electron transfer to leave regions of cations and anions on surfaces [60]. In this study, plasma triboluminescence distributions around sliding polymer contacts in UV-vis range were measured simultaneously with surface electrostatic potential generated on the polymer. The obtained data were fed into a simplified model of electric field configuration in order to figure out the basic mechanisms of discharge ignition.

2. Test methods

A sliding contact was produced by loading a 5 mm diameter, single crystal Al_2O_3 hemisphere against a rotating polymer disc (see Fig. 1), while a UV sensitive camera (Hamamatsu ImagEM X2) with UV-13X lens (Newport) was focussed through the Al_2O_3 specimen (Swiss jewel, USA) onto the contact to obtain images of the generated plasma luminescence. A charge sensor (of the type developed in Ref. [61]) was positioned diametrically opposite the contact with its tip 2 mm above the disc surface and was connected to an electrometer (Keithley 6517B) to record the accumulated charge signal. For certain tests, the camera was replaced by a spectrometer (Ocean Optics QE Pro) to measure the optical spectra of the plasma. All tests were carried out at 2 N load (corresponding to the initial average Hertzian contact pressure of 40 MPa for PTFE and 16–52 MPa for UHMWPE) and 2.4 m/s sliding speed. After each test, scans of the specimen surfaces were performed using a variable pressure SEM (pressure of 60 Pa, 15 kV beam voltage and ×100 magnification) and a Veeco optical profilometer.

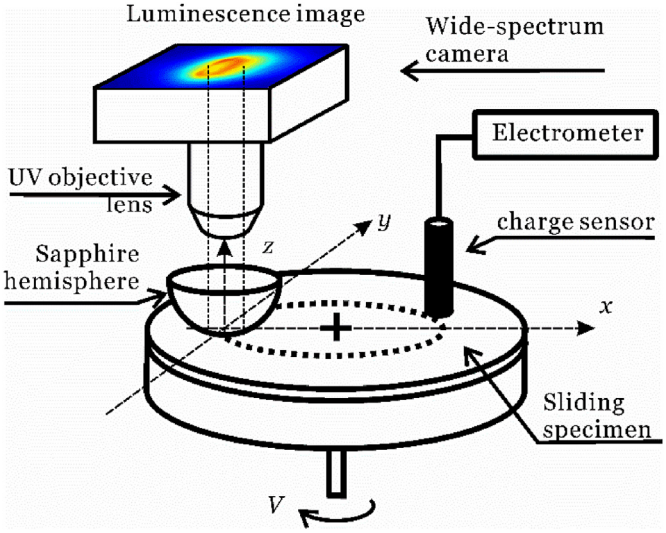

Fig. 1. Schematic diagram of test set up showing the sliding contact between Al_2O_3 hemisphere and polymer disc.

Test specimens were discs of UHMWPE and PTFE (Goodfellows, UK). The crystallinity of polymer samples was measured using X-ray diffraction and found to be 54% and 40% for UHMWPE and the PTFE respectively. Single crystal alumina (Al_2O_3) was used for the stationary specimen, since it is transparent to UV and visible wavelengths and enables plasma discharge within the contact to be viewed. All tests were conducted in an ambient atmosphere and room temperature and relative humidity varied between 20 and 50%.

3. Results and discussion

3.1. Experimental transient plasma measurements

Fig. 2 shows time-averaged plasma luminescence intensity images, recorded during rubbing tests on the PTFE and UHMWPE specimens with a frame rate of 1.2 fps for 120 s. The shapes of the triboplasma regions generally agree with those obtained by Nakayama for single crystal oxides (*e.g.* Refs. [41,51]): for PTFE, the luminescence zone has an almost circular geometry with a reasonably uniform luminosity distribution, whereas for UHMWPE it is elongated. Weak protrusions along the wear track at both the inlet and exit sides can be distinguished. For PTFE, a bow-shaped glow is observed around the contact zone that extends to a point approximately 200 μm behind it. This corresponds to Miura's β-peak (the location past the exit of the contact where the geometry of the gap and the configuration of electric field provide a maximum propensity for discharge) [42]. For UHMWPE, a peak is observed in front of the inlet of the contact. This resembles Miura's γ-peak (the location before the inlet of the contact where re-entering charge and gap geometry provide a maximum propensity for discharge) [42], however, it is located closer to the contact zone. In addition to this, both polymers show weak luminescence at the contact areas (Miura's α-peak). Overall, these findings are broadly in line with the work of Nakayama [51] who found that UV luminescence image became symmetrical with respect to the radial axis when a relatively

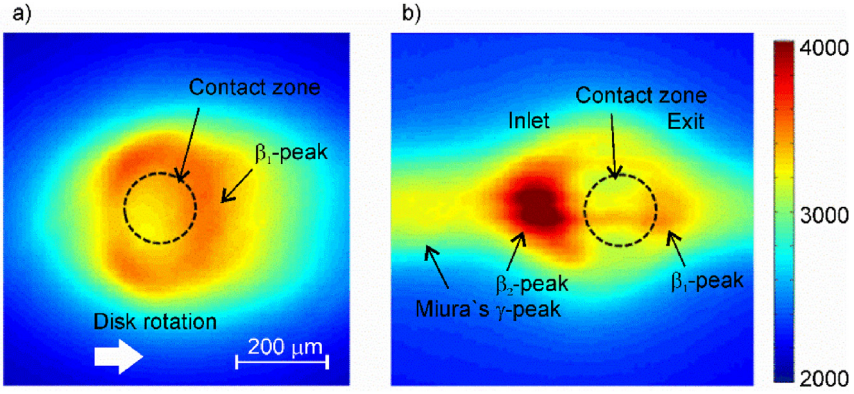

Fig. 2. Measured luminescent zone configuration, from a) PTFE contact, b) UHMWPE contact.

blunt diamond pin (3 mm radius) was used. Thus, it can be suggested that increasing the pin radius promotes symmetrical luminescence shape. The size of the luminescent region for both polymers is about an order of magnitude larger than Nakayama's, which we attribute to our more compliant specimens producing a smaller gap between the specimens, and extends the region where gas discharge can exist away from the contact (note that PTFE image has been cropped to enable comparison).

Fig. 3 shows the spatial luminescence of PTFE and UHMWPE, varying over a millisecond timescale, obtained at a frame rate of 70 fps. This behaviour is highly dynamic with the intensity and position of the described features varying substantially with time. The frames taken at 14 ms correspond to the moment just before the discharge ignition. The images in Fig. 3a) for PTFE recorded at 28–56 ms show a sequence of small discharges made up of burst pulses at and around the contact zone. From 56 ms onwards, intensive spots at the exit and the inlet of the contact zone appear, denoted as β_1 and β_2, correspondingly. A tail spreading behind the peak β_1 along the wear track breaks the symmetry of the luminescent zone, although, a symmetric weak protrusion in front of β_2 appeared in some pictures. This splitting of the β peak into two symmetrical peaks has not been observed for the combinations of sliding materials and sharp pins studied by Nakayama [41–43]. After approximately 10 s of sliding, the luminescence intensity decreases and its pattern becomes asymmetric, as presented in Fig. 3b. It is no longer spread around the entire contact zone, but consists of burst pulses some of which are short and bow-shape and situated close to the contact zone, while others with varying irregular shapes protrude outwards (see a video recording S1 in Supplementary materials).

Supplementary video related to this article can be found at https://doi.org/10.1016/j.triboint.2018.09.026.

UHMWPE luminescence (shown in 3c) consists of branched streamers with only a small contribution from burst pulses. The streamers propagated in all directions, although, they are more frequent at the inlet side of the contact zone (Fig. 3c). Bright spots at the periphery of the contact zone (see frames at 100 ms, 112 ms, 141 ms, and 155 ms) are seen when electrons of the streamers approached the pin. The luminescence behaviour does not change considerably with sliding time (see video record S2 in Supplementary materials).

Supplementary video related to this article can be found at https://doi.org/10.1016/j.triboint.2018.09.026.

These two forms of discharge *i.e.* burst pulses and streamers, have not been observed previously, since earlier studies [41,42,45,50–53] have only presented time-averaged images (longer exposure times were required due to the low levels of emitted light). With respect to this, it should be noted that apart from the observed dynamic behaviour on a millisecond timescale, most discharges are known for being inherently pulsating on the microsecond timescale, where frequency increases with the increasing potential [62,63], while the duration of the individual streamers in nitrogen is between several tens and a hundred of microseconds [64]. Although the time resolution of our experimental set-up (14 ms) was not sufficiently small to observe the development of individual streamers our results give clues for the correct understanding of the time-averaged luminescence images such as those shown in Fig. 2 and presented in earlier studies [41,42,45,50–53]. In fact, those images must be interpreted in terms of photon emission probabilities: the higher the luminescence intensity at a certain point, the higher is the likelihood to observe photon emission at this point due to various intermittent discharge processes and events. There is a direct analogy in the representation of time-averaged luminescence and electron orbitals, both of which are density functions of the probability of having photon or electron, respectively, although on different scales. This approach contrasts the established view that time averaged images of triboluminescence are still images of a distributed gas discharge, *e.g.* glowing discharge in a tube between parallel electrodes. For example, the intensive β_2 peak in Fig. 3a, does not signify a glowing crescent-shape but is instead due to bursts and streamers more likely occur in this zone. A higher degree of symmetry of luminescence images for PTFE indicates that bursts and streamers do not have preferential direction.

The marked differences between the two materials are evident from the time series of maximum plasma intensity in Fig. 4. In this figure, each data point represents the maximum intensity in consecutive camera frames acquired at the rate of 1.2 Hz. After a sharp initial peak, PTFE shows a significant and monotonous decrease in luminescence intensity. For UHMWPE (Fig. 4), the behaviour is chaotic and consist of sporadic sharp bursts on a relatively low-level base luminescence. The intensity of the base luminescence is similar to the intensity of steady luminescence for PTFE. The maximum burst intensity for UHMWPE is, however, only about one-third of the initial luminescence intensity for PTFE.

The triboluminescence spectra were obtained from both UHMWPE and PTFE and found to be alike in structure, although the former is less intensive and with higher dispersion due to its inherently unstable plasma behaviour. Fig. 5 shows a portion of the emission spectrum measured on PTFE. The spectra are dominated by the bands of the second positive system of N_2 ($C^3\Pi_u - B^3\Pi_g$) corresponding to $\Delta\nu = \nu'\text{-}\nu''$ from 2 to −4, where ν' and ν'' are vibrational quantum numbers of $C^3\Pi_u$ and $B^3\Pi_g$ metastable electronic states, respectively [65–67]. Some weak contributions from the first positive system of N_2 (503–800 nm), the first negative system of N_2^+ (329–587 nm) and emission bands of atomic N and O can be noticed [68]. Rotational bands were not resolved. The vibrational temperature of plasma was deduced using the Boltzmann plot method under the assumption of plasma being optically thin, and local temperature equilibrium (for time > 1 μs) [69]. To determine the intensities of various superimposed bands, the measured spectra were fitted with Gaussian peaks, with centres fixed at the positions of $\nu'\text{-}\nu''$ transitions for N_2 $C^3\Pi_u - B^3\Pi_g$ [70]. The adjusted coefficient of determination was higher than 0.995. Then, the transitions $\Delta\nu = 2$ (4-2), $\Delta\nu = 1$ (3-2, 2-1, 1-0), $\Delta\nu = 0$ (0-0, 1-1, 4-4), $\Delta\nu = -1$ (2-

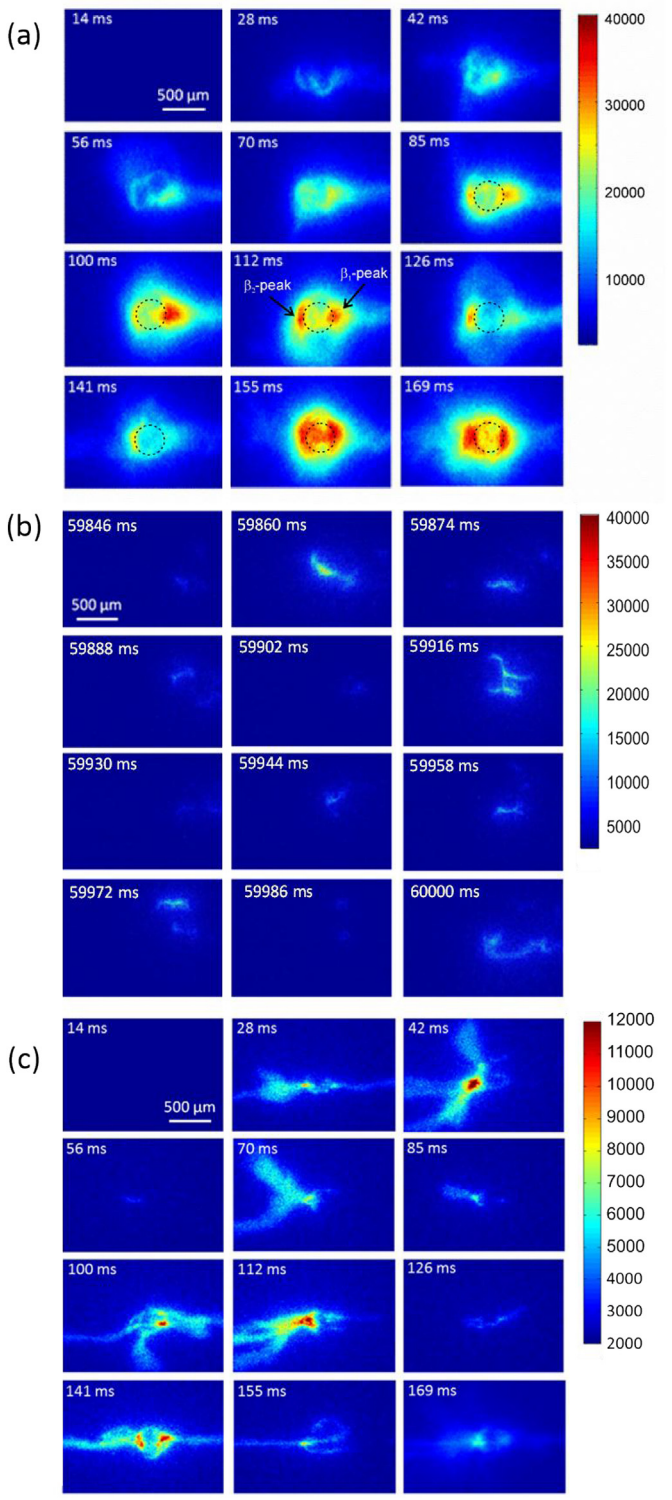

Fig. 3. Images of transient plasma distributions (sliding direction from left to right), obtained with a frame rate of 70 Hz for a) PTFE: during first few seconds b) PTFE: during the remainder of the sliding period and c) UHMWPE.

3, 1-2, 0-1), $\Delta\nu$ = -2 (0-2, 1-3, 2-4, 3-5, 4-6), $\Delta\nu$ = -3 (0-3, 1-4, 2-5, 3-6, 4-7), and $\Delta\nu$ = -4 (0-4, 1-5, 2-6, 3-7) were used for drawing a Boltzmann plot. The radiative transition parameters: the Einstein coefficient, the wavelength, the statistical probability and the energy of the upper energy level, which are required for calculation, were taken from NIST atomic spectra database and other available literature [67,70]. The adjusted coefficient of determination of a linear fit of the experimental

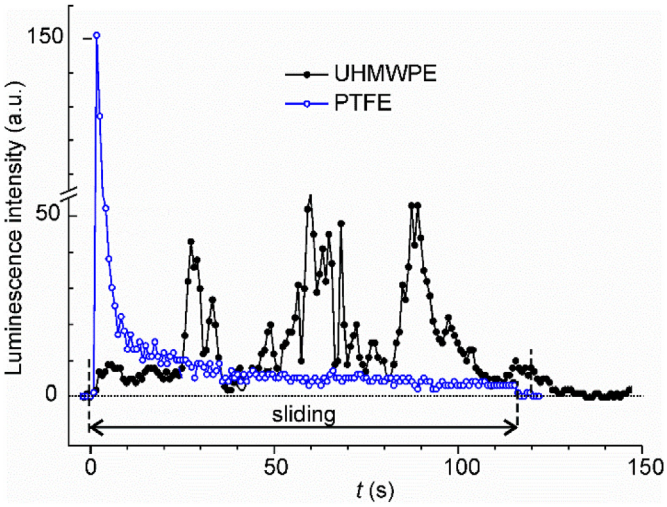

Fig. 4. Maximum transient triboplasma intensity vs. time for PTFE/Al_2O_3 and UHMWPE/Al_2O_3 contacts.

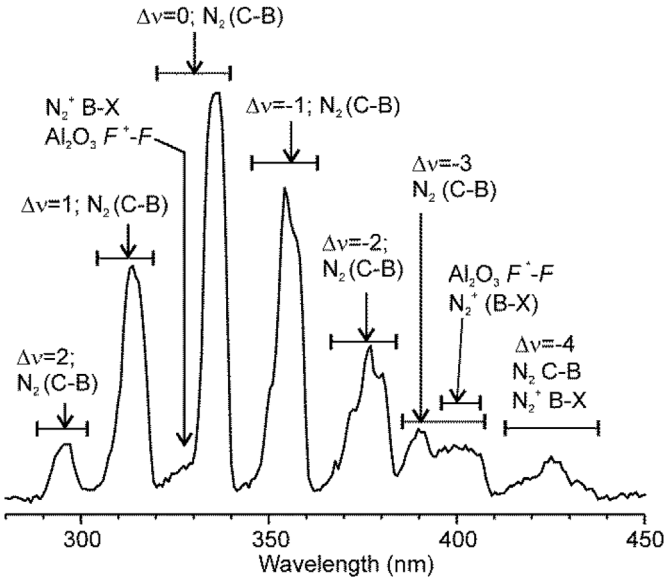

Fig. 5. A portion of plasma emission spectra in the range of wavelengths 280–450 nm for PTFE sliding contact.

Table 1
Parameters used for contact temperature calculation.

	Sapphire pin [74]	PTFE disc [75]
Thermal conductivity (W m^{-1} K^{-1})	48	0.25
Heat capacity (J $kg^{-1}K^{-1}$)	761	1000
Young modulus (GPa)	345	0.3–.8
Poisson's coefficient	0.28	0.46
Friction coefficient	0.1	
Normal load (N)	1.4	
Sliding velocity (m s^{-1})	2.8	
Radius of contact zone[a] (μm)	124	

[a] Calculated from elastic Hertzian model.

data was 0.523. Vibrational temperature determined from the slope of the Boltzmann plot was 6405 K with a standard error of 1251 K. This value contrasts the (flash) temperature increase in the contact, which was calculated for PTFE/Al_2O_3 sliding using Kennedy's method [71] (inputting the parameters shown in Table 1) and found to be 17.3 °C above ambient (and confirmed with IR camera measurement of 14 °C).

This temperature rise is equivalent to 1.5 meV and is not very different from the finding of Nakayama for diamond/sapphire sliding [72] considering that thermal conductivity of sapphire disc is nearly two orders of magnitude higher than for PTFE. Considering that infra-red emission corresponds to the temperature of heavy particles such as neutrals and ions, our findings give evidence of highly non-equilibrium conditions in tribologically induced plasmas. Such conditions usually take place in low-temperature plasmas at low electron energies, when elastic scattering is the most frequent [73]. Vibro-electronic excitation and ionization are less frequent and have a range of energy thresholds. The presence of low density of ions in the triboluminescent zone is evident from the weakness of the bands of N_2^+. For various gases, the bands of ionized species in triboluminescence spectra were usually lacking, although the bands of metastably excited neutrals were almost identical to the spectra of glowing discharge [53]. This finding supports the hypothesis put forward by Nevshupa [38] that for non-symmetrical configurations such as pin on disc, the type of gas discharge is corona dominated by the electric field of the pin rather than bipolar glowing. These results also show that a part of the mechanical energy that is transformed into electric field at the sliding contact is coupled mainly to the electrons and is related to the selective production of reactive species including electronically and vibrationally excited molecules, positive and negative ionic species, radicals, photons etc. The energies of these excited species range between several and several tens of electron-volts, which is several orders of magnitude higher than the vibrational energy due to frictional temperature increase (1.5 meV).

There are certain features of the break down spectra, which cannot be attributed to N_2 breakdown. The two weak bands centred at 334 nm and 400 nm could originate from luminescence of F^+ and F^* centres in sapphire [76,77]. In this work, the sapphire pin became charged positively and acted as an anode, so emission of these bands could be excited by electron impact in addition to photoluminescence due to ultraviolet radiation. Furthermore, the shape of the bands at 400 and 425 points at the possible contribution from non-nitrogen radicals, *e.g.* CH, which can arise from polymer bond scission and triboemission of volatile alkanes [78].

3.2. Effect of surface charge

The next test involved recording the time series of the accumulated surface charge, measured using the electrometer alongside the plasma intensity, as shown in Fig. 6. At the beginning of sliding, the charge density increases linearly. The initial rates of charge accumulation are 49.6 and 11.0 $nCm^{-1}s^{-1}$ for PTFE and UHMWPE, respectively, as determined from the slope of the plot in Fig. 6c. A deviation from the linear behaviour is observed at approximately 1.5 s (PTFE) and 6.5 s (UHMWPE) which coincides with the discharge ignition. The linear charge densities at the moment of discharge ignition are 55.6 and 34.0 nCm^{-1} for PTFE and UHMWPE, respectively. After discharge ignition, the surface charge density varies slowly with time and tends to stabilize. For UHMWPE, steady state is reached in less than 100 s, whereas for PTFE the charge accumulation continues at a low rate. In addition to this, the steady charge density for PTFE is significantly more negative than for UHMWPE, which can be related to much higher electronegativity (4.0) and electron affinity (328 kJ/mol) of fluorine in comparison with carbon (2.5 and 121.7 kJ/mol, correspondingly) and hydrogen (2.2 and 72.8 kJ/mol, correspondingly).

Stabilization of the surface charge density indicates that the rates of charge generation and recombination are close to equilibrium. If the rate of charge generation is considered constant during the whole experiment, the amount of charge dissipated in time t can be found from the difference between the instant measured value of the surface charge density and the value found from the extrapolation of the initial linear part of the graph (Fig. 6b). This suggests that a significant part of the generated charge is dissipated through the gas discharge and the electric current feeding the gas discharge can be estimated from the rate of

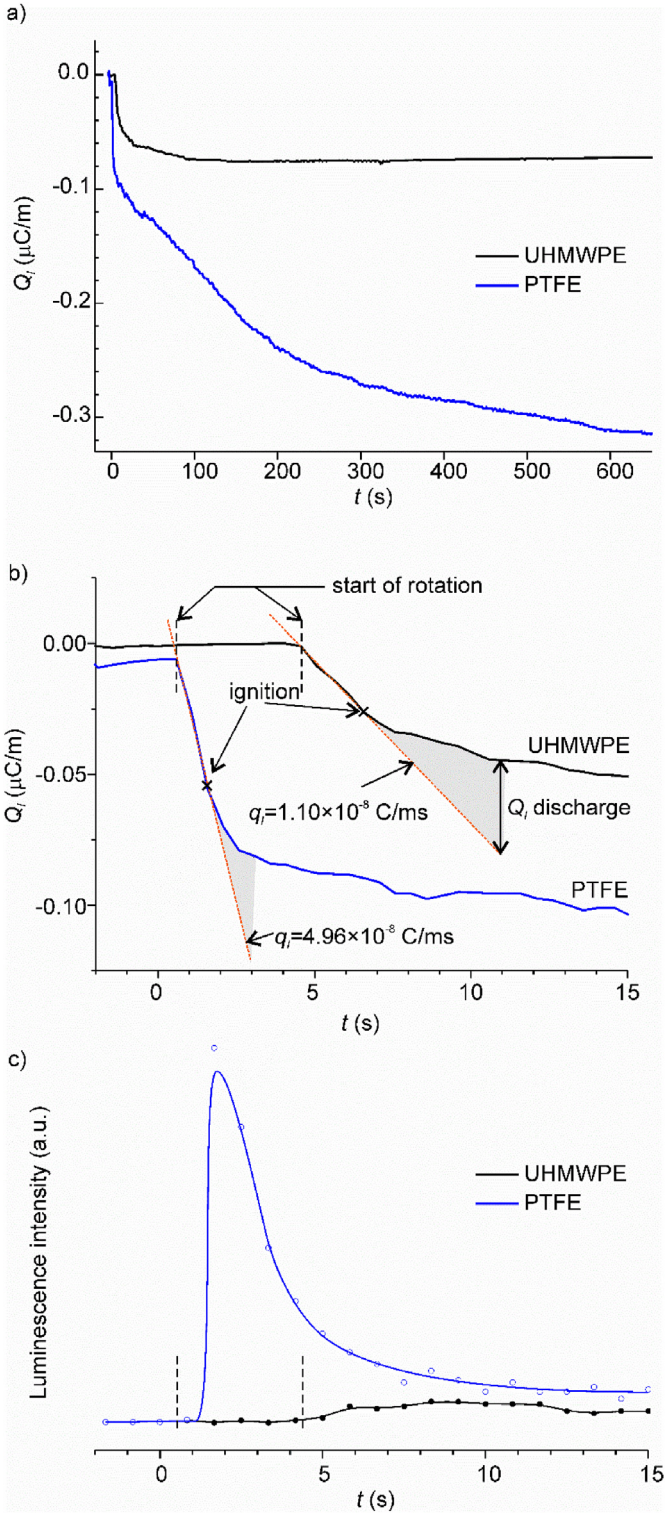

Fig. 6. (a) Variation of surface charge density as a function of time. b) Enlarged portion of the plots of charge density showing initial linear behaviour. Straight lines are linear fits. Vertical dashed lines mark the rotation beginning. (c) Initial part of the plot of the maximum luminescence intensity for PTFE and UHMWPE sliding against Al_2O_3.

charge generation, q_j:

$$I_d \approx q_j \pi d \tag{1}$$

where d is the diameter of the wear track.

For d = 40 mm, (1) yields 69.9 nA and 42.7 nA for PTFE and

UHMWPE, respectively. It should be stressed that for UHMWPE, instant current during bursts can be significantly higher, since, the charge is measured on the disc surface away from the contact and therefore gives no indication of the charge on the Al_2O_3 hemisphere specimen. However, the total amount of charge dissipated at the pin and at the disc by time t should be very similar. In this rough estimation, we assumed that gas discharge is the only mechanism of charge dissipation and recombination. If this were the case, then the plasma luminescence signal would increase or at least remain constant throughout the test, whereas in actuality, it reduces rapidly. Therefore, in the real situation, some other processes must be occurring in parallel, to reduce the surface charge to a value below this estimated upper bounds. One such process is the transfer of negatively charged material from the PTFE disc onto the positively charged alumina hemisphere, which is a known lubrication mechanism for this polymer [79,80]. In other words, as sliding commences, PTFE particles trapped in the contact are sheared leading to bond scission and the formation of ions [60] on the polymer surface. This results in tribocharging, as regions of negative fluorocarbon ions accumulate on the polymer surface. However, this shearing process also results in the adhesive transfer of PTFE from the disc to the alumina surface so the interface transitions from being PTFE/Al_2O_3 to PTFE/PTFE (as confirmed later by SEM), so the density of negative charges on the disc and positive charges on the pin decreases.

The differences in behaviour between the time series of luminescence intensity (Figs. 4 and 6c) and surface charge density (Fig. 6a), which can be seen on a large time scale (tens and hundreds of seconds), are not surprising since the charge measured on the disc away from the plasma region gives an indication of the efficiency of surface charge recombination in plasma rather than on the rate of tribocharging. So, a gradual increase of charge density on PTFE implies either incomplete recombination of charges in plasma or charge leakage out of the wear track due to debris transfer or charge diffusion. The latter process can be intensified under UV radiation [49]. In turn, the brilliance of triboplasma is a function of the current density passing through the plasma which depends on the rate of charge generation and configuration of the electric field. The rate of charge generation can be affected by the surface conditions and material transfer which is discussed in the next section. The electric field can also be distorted due to the build-up of local space charge around the pin due to the accumulation of positive and negative ions in the air that can even completely choke the discharge. Furthermore, attachment of charged polymer debris can locally reduce electric field strength, increase tortuosity of the path of electrons towards the anode and cause breaking of symmetry in the luminescence pattern. In the case of UHMWPE, although steady surface charge did not give indications of any considerable charge leakage, the rate of charge generation may be insufficient to establish a steady gas discharge. Another important factor controlling the type of discharge is the availability of seeding electrons since electron emission from a cathode by ion impact is negligible under the given experimental conditions and configuration of the discharge zone. UHMWPE should produce a higher rate of electron emission, than PTFE, due to its much lower electron affinity. Therefore, the chance of streamer development should be higher for UHMWPE, which is consistent with the observed plasma behaviour on microsecond scales.

3.3. Effect of friction and wear

In Fig. 7, a comparison of luminescence intensity, friction coefficient and wear depth during PTFE/Al_2O_3 sliding tests is shown. Friction remains approximately constant throughout the test, while photon emission intensity varied by a factor of seven. Although wear rate (depth) is highest during the first 2 s compared to the later stages (due to reducing contact pressure), it is not proportional to the observed plasma intensity variations. This does not, however, preclude the indirect influence of wear, since a number of studies [28,30,31] have

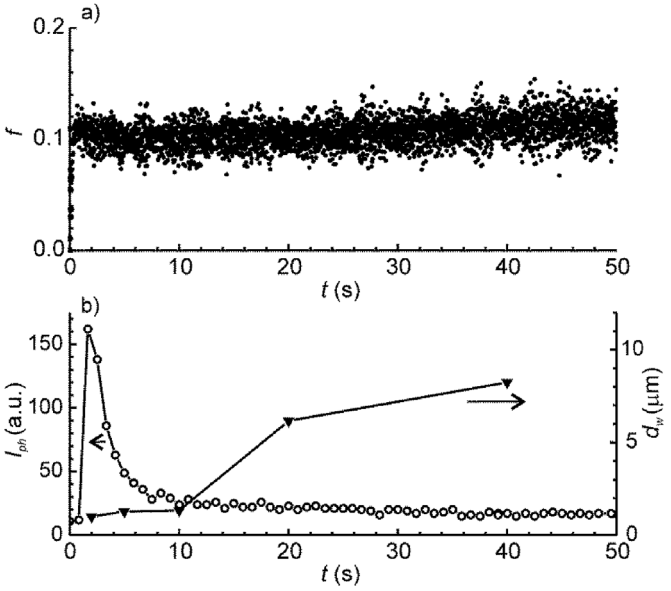

Fig. 7. Variation in a) friction coefficient (f), b) wear depth (d_w) and maximum emission intensity (I_{ph}) with time for PTFE/Al_2O_3 contact, loaded with 1.4 N and sliding at a speed of 2.8 m/s.

suggested that charging behaviour is governed by material transfer between specimens, which can be independent of wear rate.

To test the hypothesis that material transfer influences the variation in plasma and charging, repeat tests were performed on the same wear track (Fig. 8a), showing that emission resumes only after PTFE transfer film and debris have been removed from the alumina specimen. This

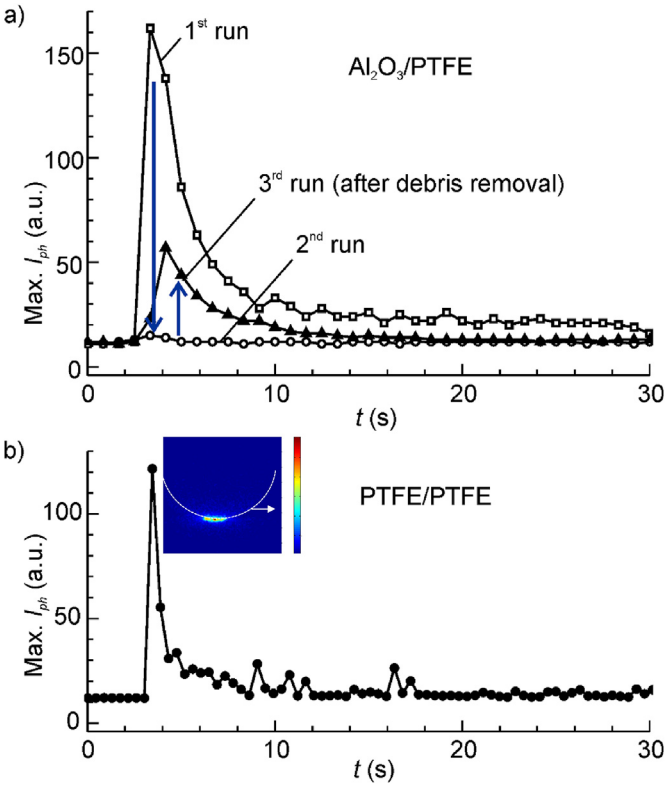

Fig. 8. Variation in maximum emission intensity (I_{ph}) with time for (a) PTFE/Al_2O_3, showing the effect of repeated tests on the same track and debris removal. (b) PTFE/PTFE contact, loaded with 1.4 N and sliding at a speed of 2.8 m/s (inset shows the side image of luminescence).

strongly supports the idea that the reduction in plasma observed during the PTFE test could be caused by charge equalisation due to predominantly negatively charged debris transferring to the positively charged hemisphere surface. This can also be responsible for the change in the pattern of burst pulses with sliding time. The 65% reduction in emission between the test on the new and cleaned wear track can conceivably be attributed to the decrease in contact pressure due to wear as the contact becomes increasingly conformal with a larger contact area with the grooved wear track.

To further investigate the mechanism of charge generation, a test was run in which a PTFE ball loaded against a PTFE disc. Since PTFE is opaque, this precluded viewing of the contact through one of the specimens and therefore the UV-camera was positioned to the side of the contact. An example of the images obtained in this way is shown in the inset in Fig. 8b, while the rest of the figure shows the variation in maximum plasma luminescence intensity over time. It is striking that this plasma variation for the PTFE/PTFE contact is nearly identical to that of the PTFE/Al_2O_3 contact. This shows that shearing of the PTFE leading to molecular scission must be the mechanism responsible for charging, (since electron transfer mechanisms due to contact potential difference can be discounted for charging contacts consisting of identical materials).

Fig. 9 shows SEM images of the specimens obtained after each test, where clear differences can be observed between the two polymer materials. Focusing first on the transfer of polymer to the pin specimen, Fig. 9a shows PTFE debris having been transferred from the disc to the hemisphere, which is present *inside* the contact area. Fig. 9c, on the other hand shows a UHMWPE transfer film on the Al_2O_3 hemisphere *outside* the contact area on the exit side. This may hamper the establishment of steady gas discharge and explains the unusual configuration of the luminescent zone with the maximum intensity at the inlet of the contact zone for the UHMWPE (Fig. 2), since the transfer of polymer material to the hemisphere at the exit would reduce the strength of the electric field. It is also important to note that the transfer of UHMWPE to the Al_2O_3 hemisphere must first occur *inside* the contact area before being transported to the exit due to the high shear stress within the contact. This building up and subsequent removal of material within the contact is a probable cause of the luminescence intensity fluctuations observed in Fig. 4.

Now considering the morphology of the PTFE and UHMWPE wear tracks, shown by the SEM images in Fig. 9b and d. In the case of PTFE, flat lamellar flakes, similar to those found on the Al_2O_3 hemisphere, can be observed embedded in the wear track (in agreement with [80]). The UHMWPE, however, shows more fibrous debris, approximately half the size of the PTFE, appearing stretched in the direction of sliding. (See Supplementary information S3 showing motion and accumulation of debris in-situ at the sliding contacts for PTFE and UHMWPE recorded using a camera).

The contrasting wear behaviours of the two polymers can be attributed to their molecular structures, morphology, crystallite size and its orientation. UHMWPE consists of very long, highly cross-linked molecular chains, which improve its wear resistance [81]. It has a low glass transition temperature of around −150 °C and a higher crystallinity of 54% compared to PTFE (40%). UHMWPE also has higher yield stress (0.2–1.2 GPa compared to 0.3–0.8 GPa [75]). The high strength and propensity to flow explains the observed fibrous morphology of the UHMWPE wear track as well as the adhered deposits on the Al_2O_3 hemisphere, which occur in response to the high shear stress and moderate temperature in the contact. PTFE, on the other hand, has low wear resistance that is closely associated with the smooth profile of the rigid-rod-like PTFE molecule [80] and a higher glass transition temperature of around 115–130 °C [82]. This explains the PTFE's wear

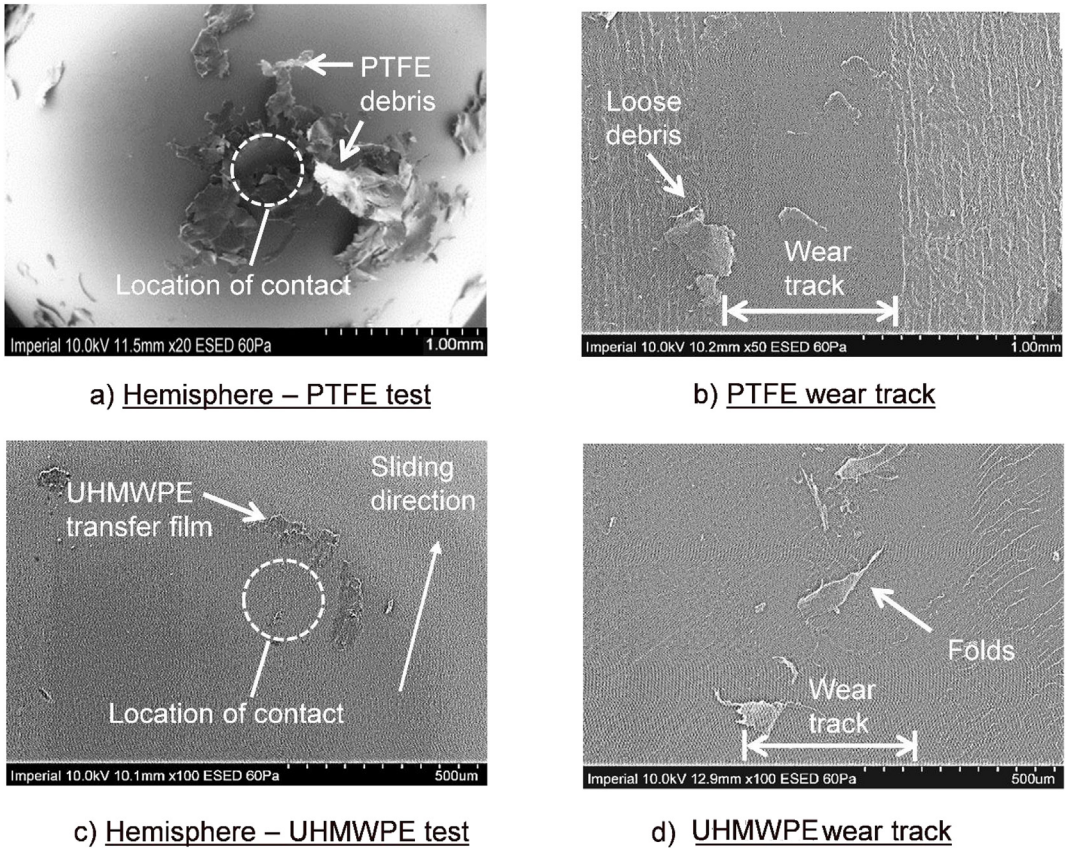

Fig. 9. SEM images of a) charged PTFE debris attached to Al_2O_3 hemisphere, b) wear track on PTFE disc, c) UHMWPE transfer film on Al_2O_3 hemisphere, d) wear track of UHMWPE.

track morphology, since it is less cohesive and tears more easily to form lamellar flakes, which become embedded in the wear track during subsequent rotations. This wear process initially generates charge due to the scission of molecules (a process demonstrated by the fact that a PTFE-PTFE contact generates similar luminescence behaviour to the $Al2O_3$-PTFE contact). However, the greneration of flakes is known to be a self-limiting process since once formed, they shear easily and prevent subsurface rupture [83] and generation of charged radicals [84]. This wear behaviour perfectly explains the rapid increase and subsequent decrease in charge rate and plasma generations observed in Figs. 3, and 5 to 8.

There is also the possibility that the pressure and temperature at the contact zone (calculated above to be around 40 MPa and 42 °C respectively) could cause phase transitions of PTFE from hexagonal to disordered pseudo-hexagonal or triclinic crystalline structures [85,86]. To our knowledge, the effect of phase transitions on the tribocharge generation of PTFE has not been studied so far, but it cannot be discarded.

3.4. Model of electric field configuration and the onset of discharge

The configuration of the electric field just before discharge ignition was modelled using a finite element method following the approach described in Ref. [38]. The upper, flat surface of the hemispherical pin and the bottom face of the polymer disc were grounded. The pin and the disc were set inside a conductive grounded cylinder filled with air. Mean surface charge density on the disc was calculated from the experimentally measured linear charged density, assuming the constant width of the wear track 600 µm. The charge accumulated on the pin was assumed being equal the total charge on the disc surface, but with opposite sign. It was also assumed that positive charge is uniformly distributed over the circular contact area of the pin tip which has diameter 600 µm. Charge diffusion, leakage or recombination were not considered. Simulation was made for the moment just before discharge ignition (Fig. 6b). Linear charge density, Q_l, surface charge density, Q_s, and the total accumulated charge, Q, for the disc and the pin are shown in Table 2.

The simulated radial and axial components of electric field on the disc surface along axis x and z, correspondingly, are shown in Fig. 10a. Despite considerably different charging rates, the strength of the electric field at the discharge ignition for PTFE and UHMWPE are quite similar. For both polymers, the radial component is nearly an order of magnitude higher than the axial component. The weak electric field of the charged wear track caused only little variation in radial and axial components of the electric field along y-direction in comparison with x-direction. Therefore, the total electric field is dominated by the highly stressed anode (Al_2O_3 hemisphere), which has concentrated positive charge over a small surface contact area. Because of the confined geometry of the gap between the pin and the disc, the electric field is quite uniform across the gap along $z$direction, but has a strong gradient in the radial direction. Our model, therefore,suggests that the electric discharge is of a positive corona type, which contradicts the earlier models based on the assumption of the electric field directed across the gap leading to bipolar gas discharge [51,52]. Fig. 11a schematically shows the processes leading to the ignition of gas discharge and the appearance of luminescence.

Table 2
Linear charge density, Q_l, surface charge density, Q_s, and the total accumulated charge, Q, for the disc and the pin just before ignition of the discharge.

	Disc			Pin	
	Q_l (C m^{-1})	Q_s (µC m^{-2})	Q (nC)	Q_s (µC m^{-2})	Q (nC)
UHMWPE	-3.40×10^{-8}	−56.7	−4.3	1500	4.3
PTFE	-5.56×10^{-8}	−92.7	−7.0	2470	7.0

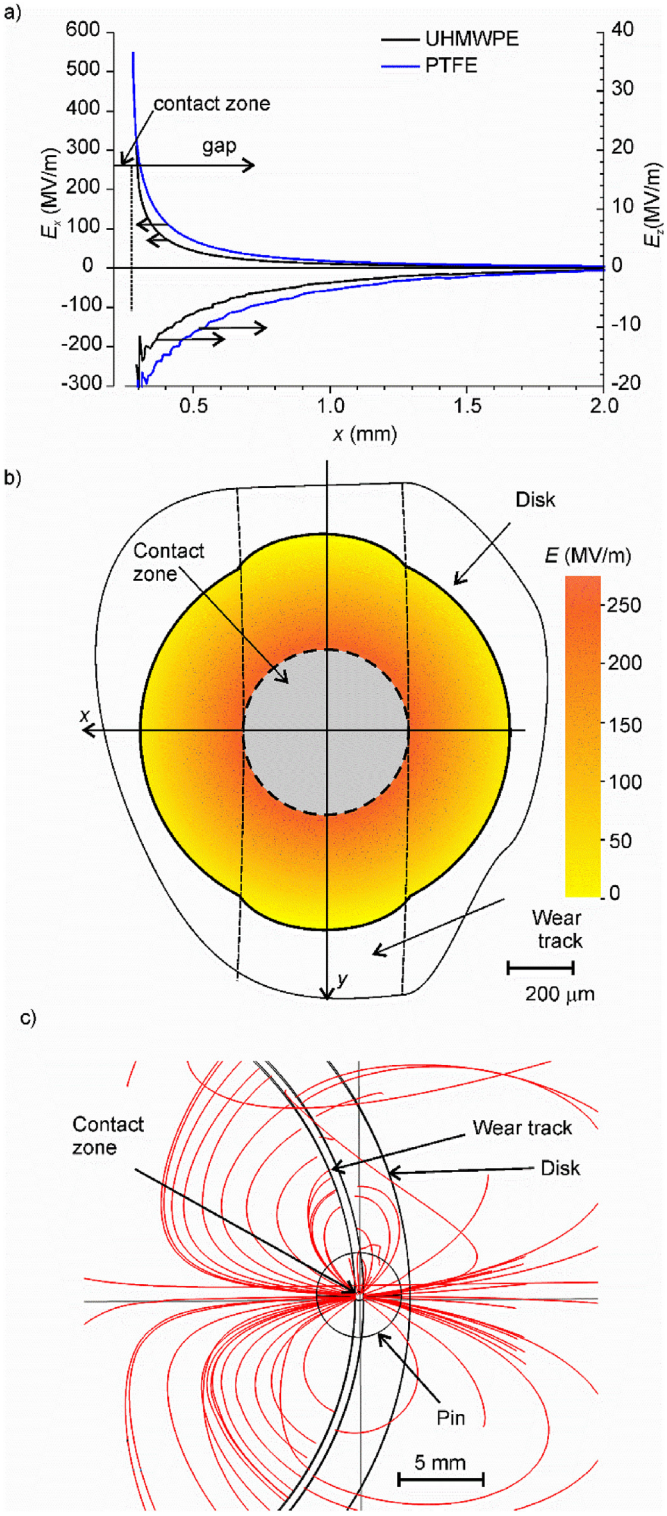

Fig. 10. Simulation results just before breakdown: a) radial (E_x) and axial (E_z) components of the electric field for the two polymers. b) the coloured region shows the zone for PTFE/Al_2O_3 sliding where conditions for breakdown are easiest. c) lines of the electric field around the contact zone for PTFE/Al_2O_3 sliding.

The conditions for breakdown are easiest at Stoletov's point, E_s, where the ionization capability of electrons is at a maximum. For air at atmospheric pressure, this corresponds to $E_s = 27.4$ MV/m [63,87]. The zone where the electric field, E, at the moment of ignition satisfies the following condition:

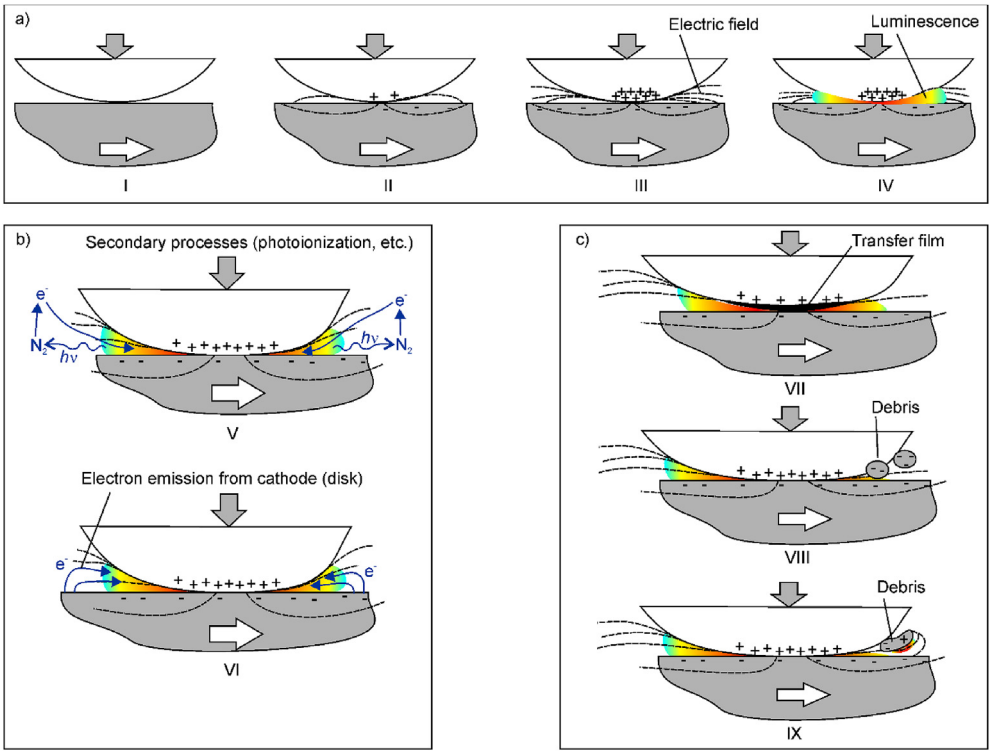

Fig. 11. Schematic representation of various processes relevant to triboluminescence at Al_2O_3/polymer sliding. a) Initial electric field build-up and discharge ignition, b) secondary process, c) Relevant tribological processes.

$$E \geq E_s \tag{2}$$

and is shown in Fig. 10b by coloured zone. The colour map indicates the strength of the electric field. For discharge ignition at these conditions, the minimum thickness of the air layer around the anode should be 11 μm (this distance must be measured *along* the gradient ofthe electric field that is in the radial direction and *not across* the gap). The width of the coloured zone surrounding the contact zone is about 250 μm so the required condition for the minimum distance is fulfilled. The shape and the size of the coloured zone in Fig. 10b, are quite similar to that of the experimental time-averaged images of luminescence (Fig. 2), which confirms that luminescence occurs in the region, where condition (2) is satisfied, and also supports our hypothesis about the configuration of the electric field. It should be stressed, that in our simple model no assumption on the charge diffusion from the contact zone was made. The configuration of the electric field is governed only by the local charge on the contact zone. This contrasts some previous approaches in which spherical pin and disk were assumed conductive with a constant potential difference applied between them [88] that led to a nearly uniform electric field across the gap. For positive corona discharge, triggering electron emission and secondary processes are of critical importance for sustainability. Furthermore, for positive corona, the cathode does not furnish a secondary mechanism of free electron emission, which therefore must be achieved due to photoionization and collisions of excited and neutral atoms [62]. Electrons produced due to photoionization within the zone of the easiest breakdown or at the distance up to 11 μm from it will contribute to the sustainability of the discharge (process V in Fig. 11b). There are a number of other possible sources of the necessary seeding electrons. For instance, when insulators are rubbed together, numerous studies have shown that this can cause surfaces to emit electrons [89,90], with various proposed mechanism such as fracture [91], field emission [92], thermal emission [93], strain relaxation [94] (process VI in Fig. 11b). UV radiation from gas discharge can also enhance electron release through photoemission. The measurements of these frictionally stimulated electron emissions typically show short duration bursts with similar temporal characteristics to the streamers in Fig. 3 [95–98].

It should be noted also that the axial component of electric field is negative at a distance of up to 2 mm from the contact zone, which facilitates the emission of electrons from negatively charged regions of the wear track. Released electrons will be drawn to the contact zone and can initiate streamers or feed pulse bursts. The field lines around the contact zone predicted by the finite elements approach in Fig. 10c show possible electron trajectories. At a larger distance from the contact zone (several millimetres), the electric field is not axisymmetric because of the displacement field and asymmetric configuration of the setup. These field lines have a bow shape. They begin at the wear track and end on the sides of the contact zone. This resembles the configuration of measured burst pulses of luminescence in Fig. 3b. Theconfiguration of the electric field also reveals two protrusions coinciding with the wear track caused by its weak electric field. These protrusions together with the triggering electron emission from the wear track can explain the preferential direction of the streamers along the sliding direction. The fact that luminescence can be observed at the inlet of the contact zone can be related with the re-entry of the charged disc surface. This is supported by reports of the half-life of corona charged polyethylene being *ca.* 30 h [29] and that of tribocharged PTFE being ca.60 h [58] (both under 60% RH).

Analysis of the luminescence shows that the dominating components for PTFE were pulse bursts. This indicates that the main secondary ionization mechanisms should be those of typical positive corona discharge (photoionization and collisions of neutrals and excited molecules). The absence of streamers means that electron emission from the mechanically affected zone on the disc should be hindered due to the very high electron affinity of PTFE. Lack of electron emission from PTFE can cause an overshoot of potential at the beginning of sliding [62] that leads to intensive luminescence at the breakdown. On the other hand, significant streamer component in UHMWPE luminescence suggests that UHMWPE provides considerable electron emission from the mechanically affected zone, as suggested by Hiratsuka [54].

When a streamer arrives at the anode, the strength of the electric field decreases due to both recombination of electric charges on the pin surface and space charge of positive ions and the discharge chokes itself. Then the electric field gradually rises due to continuous charging and repeated breakdown. For PTFE, the discharge behaviour is more uniform, which can be related to the higher rate of charge generation and limited electron emission from the disc surface.

Referring to the schematic drawing in Fig. 11 of the initial electric field build-up and discharge ignition, the following stages can be identified. First, there is an accumulation of concentrated positive charge at the pin tip and sparse negative charge on the disc, which leads to the build-up of a nearly axisymmetric electric field (I-III) around axis z passing through the centre of the pin normally to the disc surface. Then, when the strength of the electric field reaches the critical value corresponding to Stoletov's point, breakdown occurs. The discharge is similar to positive corona (IV) since the electric field configuration is governed by highly stressed anode (pin). b) Relevant secondary mechanisms for release of free electrons, which are necessary for sustaining the gas discharge. The cathode (disc) does not furnish a secondary mechanism through ion impact electron emission. This is achieved by photoionization of gas by UV photons emitted by plasma and collisions of excited and neutral atoms (V). Additionally, the cathode can supply free electrons from the negatively charged and mechanically affected zone through various processes including exoelectron emission, field emission, photoemission, etc. (VI). c) Some relevant tribological processes influencing gas discharge triboluminescence. Build-up of a transfer film (VII) can reduce the rate of charge generation. However, triboelectrification is not inhibited at sliding of similar materials. Attachment of negatively charged and neutral debris at and around the contact zone (VIII) decreases the strength of electric field in proximity to the pin (on one side or around the pin), where the conditions are favourable for gas discharge. In addition, the presence of debris increases tortuosity of the path for electrons towards the pin and shades the luminescent zone. When the attached debris have a mosaic pattern of charge, the local electric field can distort the electric field of the pin and produce irregular luminescence patterns (IX).

In addition to the intrinsically complex behaviour of luminescence, tribology-related processes may further modify its behaviour. The rate of charge generation can be affected by the formation of a transfer film (process VII in Fig. 11). Luminescence instabilities on the large time scale (seconds) can be to a certain extent related with partial destruction and rebuilding of the transfer layer. The debris attachment to the pin described in Section 3.3 can cause local distortion of the electric field in the discharge zone (Fig. 11b) due to their own charge of the opposite sign and displacement field (process VIII in Fig. 11c). This can lead to choking of the gas discharge at one side or around the entire contact zone. This explains the mirrored time-averaged luminescence for UHMWPE and gradual extinguishing of luminescence in the case of PTFE, which could be partially restored after debris removal. Detachment of debris may cause the transient bursts of plasma occurring at milliseconds time scales observed in Fig. 3. If debris carry mosaic charges of opposite signs the combination of the external electric field of the anode and the local electric field can give rise to local bursts at the debris or between the debris and the anode (process IX in Fig. 11c). Furthermore, opaque debris can shield the optical pathway between the luminescence zone and the camera.

It should also be considered that the ambient environment [31,32] and surface moisture is an additional complication, which affects various processes relevant to triboluminescence, in particular, the charging behaviour. It was reported that contact charging increases as the relative humidity increases from 0 to 20–40% [99,100], 10–30% [54] and then decreases at higher humidity. It has been shown that every combination of tribopair has a maximum charge at its own humidity [54]. Future work will focus on unveiling how millisecond triboluminescence behaviour and surface charging of various polymers depend upon humidity.

4. Conclusions

Until now, very little has been known about how materials discharge following contact electrification, and to address this the current study has developed a technique to image the luminescence behaviour with millisecond time resolution and sub-millimetre spatial resolution around a sliding contact. Results were interpreted using a finite element model of the electric field around the contact. As well as shedding light on how charged surfaces dissipate charge, these findings confirm that contact electrification is a tribological as well as an electrostatic process, and suggest that methods such as selecting component's mechanical properties and implementing lubrication can be used to control contact electrification and breakdown.

4.1. Time-averaged luminescence

The time-averaged image revealed a nearly symmetric shape of the luminescent zone, which was more intense at the inlet of the contact zone due to severe deformation of the polymer surface at the inlet, while the luminescence at the exit side was due to the formation reentry of the charged disc surface. Luminescence spectra for both polymers are dominated by the bands of the second positive system of N_2. Vibrational temperature determined using Boltzmann plot method from the bands of N_2 $C_3\Pi_u \rightarrow B_3\Pi_g$ was 6405 $\pm$ 1251 K. This is the first time the vibrational temperature of triboplasma was determined. It was two orders of magnitude higher than the temperature at the interface, which is indicative of cold plasma.

Both polymer discs charge negatively during sliding with the surface charge density increasing slowly as sliding continues and eventually tends to stabilize. The deviation from linear behaviour occurs due to discharge ignition process. However, the slow increase in charge density suggests that additional charges were generated after discharge ignition recombination.

Simulation of the electric field configuration revealed a nearly symmetrical distribution with respect to the axis normal to the disc surface and passing through the centre of the contact zone, which was almost one order of magnitude lower than the radial component. This suggests that gas discharge is of corona type with a highly stressed anode. The predictions of the shape and the size of the zone where the conditions for gas discharge are most favourable, (*i.e.* where the strength of electric field is equal or higher than the corresponding Stoletov's point) were shown to agree with the experimentally measured values from the luminescence zone. However, transient fluctuations in plasma that have been observed for the first time, cannot be predicted in the same way.

4.2. Transient luminescence

An important observation in this work is that previous studies may have incorrectly interpreted the time-averaged images as a steady glow from the contact owing to the long exposure times used in their measurements. In fact, as our measurements show for the first time, plasma luminescence is highly transient in nature. Hence, time-averaged images must be treated as a spatial distribution of probabilities of having photon emission.

Streamers dominated luminescence of UHMWPE while for PTFE, luminescence was mainly in form of burst pulses around a contact zone with rare streamers. These differences in millisecond behaviour between the two polymers are attributed to

(a) Differences in charging rates of the polymers and their capacity to supplying free electrons. For UHMWPE emission of electrons gives rise to branched streamers which approach the contact zone along the lines of the electric field. For PTFE, emission of electrons was inhibited because of its high electronegativity that prevented streamer formation. The discharge is sustained due to secondary

processes such as photoionization.
(b) The role of charged debris particles initiating these streamers.
(c) Tribologically-related processes such as transfer layer formation and destruction, generation of debris and their attachment to the pin that leads to a decrease in the strength of electric field and a reduced rate of charge generation (debris removal from the contact interface led to a partial recovery of luminescence).

Conflicts of interest

The authors declare no conflict of interest.

Acknowledgements

This research was supported by the UK Engineering and Physical Sciences Research Council (EP/J002100/1), with additional equipment funding provided by the Taiho Kogyo Tribology Research Foundation (11A01). RN acknowledges the support provided by the Spanish Ministry of Economy, Industry and Competitivity through the grant BIA2016-79582-R.

Appendix A. Supplementary data

Supplementary data to this article can be found online at https://doi.org/10.1016/j.triboint.2018.09.026.

References

[1] Lacks DJ, Mohan Sankaran R. Contact electrification of insulating materials. J Phys D Appl Phys 2011;44. https://doi.org/10.1088/0022-3727/44/45/453001.
[2] Wang S, Xie Y, Niu S, Lin L, Wang ZL. Freestanding triboelectric-layer-based nanogenerators for harvesting energy from a moving object or human motion in contact and non-contact modes. Adv Mater 2014;26:2818–24. https://doi.org/10.1002/adma.201305303.
[3] Yang J, Chen J, Liu Y, Yang W, Su Y, Wang ZL. Triboelectrification-based organic film nanogenerator for acoustic energy harvesting and self-powered active acoustic sensing. ACS Nano 2014;8:2649–57. https://doi.org/10.1021/nn4063616.
[4] Li A, Zi Y, Guo H, Wang ZL, Fernández FM. Triboelectric nanogenerators for sensitive nano-coulomb molecular mass spectrometry. Nat Nanotechnol 2017;12:481–7. https://doi.org/10.1038/nnano.2017.17.
[5] Kneip S. Applied physics: a stroke of X-ray. Nature 2011;473:455–6. https://doi.org/10.1038/473455a.
[6] Schein LB. Electrophotography and development physics. Springer Science & Business Media; 2012. https://doi.org/10.1007/978-3-642-97085-6.
[7] Pai DM, Springett BE. Physics of electrophotography. Rev Mod Phys 1993;65:163–211. https://doi.org/10.1103/RevModPhys.65.163.
[8] Yanar DK, Kwetkus BA. Electrostatic separation of polymer powders. Electrostatics 1995;35:257–66.
[9] Zhao P, Soin N, Prashanthi K, Chen J, Dong S, Zhou E, et al. Emulsion electrospinning of polytetrafluoroethylene (PTFE) nanofibrous membranes for high-performance triboelectric nanogenerators. ACS Appl Mater Interfaces 2018;10:5880–91. https://doi.org/10.1021/acsami.7b18442.
[10] He C, Zhu W, Chen B, Xu L, Jiang T, Han CB, et al. Smart floor with integrated triboelectric nanogenerator as energy harvester and motion sensor. ACS Appl Mater Interfaces 2017;9:26126–33. https://doi.org/10.1021/acsami.7b08526.
[11] Wang J, Wu C, Dai Y, Zhao Z, Wang A, Zhang T, et al. Achieving ultrahigh triboelectric charge density for efficient energy harvesting. Nat Commun 2017;8:88. https://doi.org/10.1038/s41467-017-00131-4.
[12] Coehn A. Ueber ein Gesetz der Electricitätserregung. Ann Phys 1896;64:217.
[13] Henniker J. Triboelectricity in polymers. Nature 1962. 474–474.
[14] Diaz AF, Felix-Navarro RM. A semi-quantitative tribo-electric series for polymeric materials: the influence of chemical structure and properties. J Electrost 2004;62:277–90. https://doi.org/10.1016/j.elstat.2004.05.005.
[15] McCarty LS, Whitesides GM. Electrostatic charging due to separation of ions at interfaces: contact electrification of ionic electrets. Angew Chem Int Ed 2008;47:2188–207. https://doi.org/10.1002/anie.200701812.
[16] Shin SH, Bae YE, Moon HK, Kim J, Choi SH, Kim Y, et al. formation of triboelectric series via atomic-level surface functionalization for triboelectric energy harvesting. ACS Nano 2017;11:6131–8. https://doi.org/10.1021/acsnano.7b02156.
[17] Forward KM, Lacks DJ, Sankaran RM. Charge segregation depends on particle size in triboelectrically charged granular materials. Phys Rev Lett 2009;102:1–4. https://doi.org/10.1103/PhysRevLett.102.028001.
[18] Lowell J, Truscott WS. Triboelectrification of identical insulators : 11. Theory and further experiments 19. 1986. p. 1281–98.
[19] Soh S, Kwok SW, Liu H, Whitesides GM. Contact De-electrification of electrostatically charged polymers. J Am Chem Soc 2012;134. https://doi.org/10.1021/ja309268n. 20151–9.
[20] Harper WR. Contact and frictional electrification. Clarendon Press; 1967.
[21] Lowell J, Rose-Innes AC. Contact electrification. Adv Phys 1980;29:947–1023. https://doi.org/10.1080/00018738000101466.
[22] Liu CY, Bard AJ. Chemical redox reactions induced by cryptoelectrons on a PMMA surface vol. 131. 2009. p. 6397–401. https://doi.org/10.1021/ja806785x.
[23] Albrecht V, Janke A, Németh E, Spange S, Schubert G, Simon F. Some aspects of the polymers' electrostatic charging effects. J Electrost 2009;67:7–11. https://doi.org/10.1016/j.elstat.2008.10.002.
[24] Diaz FA. An ion transfer model for contact charging. Langmuir 1993;9:1009–15. https://doi.org/10.1021/la00028a021.
[25] Vella SJ, Chen X, Thomas SW, Zhao X, Suo Z, Whitesides GM. The determination of the location of contact electrification-induced discharge events. J Phys Chem C 2010;114:20885–95. https://doi.org/10.1021/jp107883u.
[26] LOEB LB. THE BASIC MECHANISMS OF STATIC ELECTRIFICATION. Science 1945;102:573–6. https://doi.org/10.1126/science.102.2658.573.
[27] Terris BD, Stern JE, Rugar D, Mamin HJ. Contact electrification using force microscopy. Phys Rev Lett 1989;63:2669–72. https://doi.org/10.1103/PhysRevLett.63.2669.
[28] Baytekin HT, Patashinski AZ, Branicki M, Baytekin B, Soh S, Grzybowski B a. The mosaic of surface charge in contact electrification. Science (80-) 2011;333:308–12. https://doi.org/10.1126/science.1201512.
[29] Burgo TAL, Ducati TRD, Francisco KR, Clinckspoor KJ, Galembeck F, Galembeck SE. Triboelectricity: macroscopic charge patterns formed by self-arraying ions on polymer surfaces. Langmuir 2012;28:7407–16. https://doi.org/10.1021/la301228j.
[30] Williams MW. Triboelectric charging of insulators – mass transfer versus electrons/ions. J Electrost 2012;70:233–4. https://doi.org/10.1016/j.elstat.2012.01.001.
[31] Burgo TAL, Erdemir A. Bipolar tribocharging signal during friction force fluctuations at metal-insulator interfaces. Angew Chem 2014;126:12297–301. https://doi.org/10.1002/ange.201406541.
[32] Rezende CA, Gouveia RF, da Silva MA, Galembeck F. Detection of charge distributions in insulator surfaces. J Phys Condens Matter 2009;21:263002. https://doi.org/10.1088/0953-8984/21/26/263002.
[33] Sow M, Widenor R, Kumar A, Lee SW, Lacks DJ, Sankaran RM. Strain-induced reversal of charge transfer in contact electrification. Angew Chem Int Ed 2012;51:2695–7. https://doi.org/10.1002/anie.201107256.
[34] Budakian R, Putterman SJ. Correlation between charge transfer and stick-slip friction at a metal-insulator interface. Phys Rev Lett 2000;85:1000–3. https://doi.org/10.1103/PhysRevLett.85.1000.
[35] Krim J. Friction at the atomic scale. Sci Am 1996;275:74–80.
[36] Fabian A, Krauss C, Sickafoose A, Horányi M, Robertson S. Measurements of electrical discharges in Martian regolith simulant. IEEE Trans Plasma Sci 2001;29:288–91. https://doi.org/10.1109/27.923710.
[37] Thomas SW, Vella SJ, Kaufman GK, Whitesides GM. Patterns of electrostatic charge and discharge in contact electrification. Angew Chem Int Ed 2008;47:6654–6. https://doi.org/10.1002/anie.200802062.
[38] Nevshupa R a. Effect of gas pressure on the triboluminescence and contact electrification under mutual sliding of insulating materials. J Phys D Appl Phys 2013;46:185501. https://doi.org/10.1088/0022-3727/46/18/185501.
[39] Haynes WM, editor. CRC handbook of chemistry and physics. 96th ed.CRC Press; 2015.
[40] Thiessen PA. Physical and chemical investigations in tribomechanical events. Z Chem 1965;5:162–71.
[41] Nakayama K, Nevshupa RA. Plasma generation in a gap around a sliding contact. J Phys D Appl Phys 2002;35:L53–6. https://doi.org/10.1088/0022-3727/35/12/101.
[42] Miura T, Nakayama K. Two-dimensional spatial distribution of electric-discharge plasma around a frictional interface between dielectric surfaces. Appl Phys Lett J Appl Phys 2001;78. https://doi.org/10.1063/1.1371526.
[43] Miura T, Nakayama K. Spectral analysis of photons emitted during scratching of an insulator surface by a diamond in air. J Appl Phys 2000;88:5444–7. https://doi.org/10.1063/1.1314558.
[44] Nevshupa R, Hiratsuka K. Triboluminescence. 2015. p. 57–77. https://doi.org/10.1007/978-3-319-10560-4_4.
[45] Matta C, Eryilmaz OL, De Barros Bouchet MI, Erdemir A, Martin JM, Nakayama K. On the possible role of triboplasma in friction and wear of diamond-like carbon films in hydrogen-containing environments. J Phys D Appl Phys 2009;42:075307https://doi.org/10.1088/0022-3727/42/7/075307.
[46] Nevshupa RA. The role of athermal mechanisms in the activation of tribodesorption and triboluminisence in miniature and lightly loaded friction units. J Frict Wear 2009;30:118–26. https://doi.org/10.3103/S1068366609020081.
[47] Nakayama K, Martin J-MM. Tribochemical reactions at and in the vicinity of a sliding contact. Wear 2006;261.
[48] Nakayama K, Mirza SM. Verification of the decomposition of perfluoropolyether fluid due to tribomicroplasma. Tribol Trans 2006;49:17–25. https://doi.org/10.1080/05698190500414524.
[49] Nishi Y, Iizuka S, Faudree MC, Oyama R. Electrical conductivity enhancement of PTFE (teflon) induced by homogeneous low voltage electron beam irradiation (HLEBI). Mater Trans 2012;53:940–5. https://doi.org/10.2320/matertrans.M2011273.
[50] Muto J, Nagahama H, Miura T, Arakawa I. Frictional discharge at fault asperities: origin of fractal seismo-electromagnetic radiation. Tectonophysics 2007;431:113–22. https://doi.org/10.1016/j.tecto.2006.05.045.
[51] Nakayama K. Triboplasma generation and triboluminescence: influence of stationary sliding partner. Tribol Lett 2010;37:215–28. https://doi.org/10.1007/s11249-009-9516-5.
[52] Nakayama K. The plasma generated and photons emitted in an oil-lubricated sliding

contact. J Phys D Appl Phys 2007;40:1103–7. https://doi.org/10.1088/0022-3727/40/4/029.
[53] Nakayama K, Nevshupa R a. Characteristics and pattern of plasma generated at sliding contact. J Tribol 2003;125. https://doi.org/10.1115/1.1540122.
[54] Hiratsuka IK, Hosotani K. Effects of friction type and humidity on triboelectrification and triboluminescence among eight kinds of polymers. Tribol Int 2012;55:87–99. https://doi.org/10.1016/j.triboint.2012.05.017.
[55] Collins AL, Camara CG, Naranjo BB, Putterman SJ, Hird JR. Charge localization on a polymer surface measured by triboelectrically induced x-ray emission. Phys Rev B 2013;88:064202https://doi.org/10.1103/PhysRevB.88.064202.
[56] Kluev VA, Vladikina TN, Toporov YP, Anisimova VJ, Derjaguin BV. Emission phenomena accompanying the triboelectrification process in vacuum. IEEE Trans Ind Appl 1978;IA-14:544–6. https://doi.org/10.1109/TIA.1978.4503590.
[57] McGonigle DF, Jackson CW, Davidson JL. Triboelectrification of houseflies (Musca domestica L.) walking on synthetic dielectric surfaces. J Electrost 2002;54:167–77. https://doi.org/10.1016/S0304-3886(01)00177-2.
[58] Burgo TAL, Rezende CA, Bertazzo S, Galembeck A, Galembeck F. Electric potential decay on polyethylene: role of atmospheric water on electric charge build-up and dissipation. J Electrost 2011;69:401–9. https://doi.org/10.1016/j.elstat.2011.05.005.
[59] Burgo TAL, Silva CA, Balestrin LBS, Galembeck F. Friction coefficient dependence on electrostatic tribocharging. Sci Rep 2013;3:2384. https://doi.org/10.1038/srep02384.
[60] Beraldo da Silveira Balestrin L, Del Duque D, Soares da Silva D, Galembeck F. Triboelectricity in insulating polymers: evidence for a mechanochemical mechanism. Faraday Discuss 2014;170:369–83. https://doi.org/10.1039/C3FD00118K.
[61] Singh SV, Kusano Y, Morgen P, Michelsen PK. Surface charging, discharging and chemical modification at a sliding contact. J Appl Phys 2012;111:83501. https://doi.org/10.1063/1.3698311.
[62] Loeb L. Electrical coronas, their basic physical mechanisms. Berkeley: University of California Press; 1965.
[63] Raĭzer IP, Iurii P. Gas discharge physics. Réimpr. corr. New York: Springer-Verlag; 1991.
[64] Šimek M, Ambrico PF, Prukner V. Evolution of N $_2$ (A ^{3} $\Sigma _{{\rm u}}^{+}$) in streamer discharges: influence of oxygen admixtures on formation of low vibrational levels. J Phys D Appl Phys 2017;50:504002. https://doi.org/10.1088/1361-6463/aa96f3.
[65] Deng XL, Nikiforov AY, Vanraes P, Leys C. Direct current plasma jet at atmospheric pressure operating in nitrogen and air. J Appl Phys 2013;113. https://doi.org/10.1063/1.4774328. 023305.
[66] Lofthus A, Krupenie PH. The spectrum of molecular nitrogen. J Phys Chem Ref Data 1977;6:113–307. https://doi.org/10.1063/1.555546.
[67] Camacho JJ, Poyato JML, Díaz L, Santos M. Optical emission studies of nitrogen plasma generated by IR CO 2 laser pulses. J Phys B At Mol Opt Phys 2007;40. https://doi.org/10.1088/0953-4075/40/24/003. 4573–4573.
[68] Laux CO, Spence TG, Kruger CH, Zare RN. Optical diagnostics of atmospheric pressure air plasmas. Plasma Sources Sci Technol Plasma Sources Sci Technol 2003;12:125–38.
[69] Unnikrishnan VK, Alti K, Kartha VB, Santhosh C, Gupta GP, Suri BM. Measurements of plasma temperature and electron density in laser-induced copper plasma by time-resolved spectroscopy of neutral atom and ion emissions. PRAMANA c [Indian Acad Sci 2010;74:983–93.
[70] Gilmore FR, Laher RR, Espy PJ. Franck-condon factors, r-centroids, electronic transition moments, and Einstein coefficients for many nitrogen and oxygen band systems. J Phys Chem Ref Data 1992;21:1005–107. https://doi.org/10.1063/1.555910.
[71] Tian X, Kennedy FE. Maximum and average flash temperatures in sliding contacts. J Tribol 1994;116:167. https://doi.org/10.1115/1.2927035.
[72] Nakayama K, Yagasaki F. The temperature of triboplasma. Tribol Lett 2018;66:10. https://doi.org/10.1007/s11249-017-0955-0.
[73] Taccogna F, Dilecce G. Non-equilibrium in low-temperature plasmas. Eur Phys J D 2016;70:251. https://doi.org/10.1140/epjd/e2016-70474-0.
[74] Sapphire Properties & Material Data | Swiss Jewel n.d. http://www.swissjewel.com/materials/sapphire/(accessed February 1, 2018).
[75] Polymer - Mechanical Properties n.d. http://www.goodfellow.com/catalogue/GFCat2C.php?ewd_token=XpPnkdkV9gNjqr420971o4c3tlUoxx&n=mn7piwtGpI1iwrzRYjBQHy9hRUix9b&ewd_urlNo=GFCat26&type=30&prop=3 (accessed September 9, 2016).
[76] Lee KH, Crawford JH. Luminescence of the F center in sapphire. Phys Rev B 1979;19:3217–21. https://doi.org/10.1103/PhysRevB.19.3217.
[77] Lehmann HW, Gunthard HH. Luminescence and absorption studies on sapphire with flash light excitation. J Phys Chem Solid 1964;25:941–50. https://doi.org/10.1016/0022-3697(64)90031-9.
[78] Rusanov A, Nevshupa R, Martin JM, Garrido MÁ, Roman E. Tribochemistry of hydrogenated amorphous carbon through analysis of mechanically stimulated gas emission. Diam Relat Mater 2015;55:32–40. https://doi.org/10.1016/j.diamond.2015.02.007.
[79] Jintang G. Tribochemical effects in formation of polymer transfer film. Wear 2000;245:100–6. https://doi.org/10.1016/S0043-1648(00)00470-1.
[80] Biswas SK, Vijayan K. Friction and wear of PTFE - a review. Wear 1992;158:193–211. https://doi.org/10.1016/0043-1648(92)90039-B.
[81] Sobieraj MC, Rimnac CM. Ultra high molecular weight polyethylene: mechanics, morphology, and clinical behavior. J Mech Behav Biomed Mater 2009;2:433–43. https://doi.org/10.1016/j.jmbbm.2008.12.006.
[82] Rae PJ, Dattelbaum DM. The properties of poly(tetrafluoroethylene) (PTFE) in compression. Polymer (Guildf) 2004;45:7615–25. https://doi.org/10.1016/j.polymer.2004.08.064.
[83] Blanchet TA, Kennedy FE. Sliding wear mechanism of polytetrafluoroethylene (PTFE) and PTFE composites. Wear 1992;153:229–43. https://doi.org/10.1016/0043-1648(92)90271-9.
[84] Radtsig VA, Butyagin PY. The free radicals forming during the mechanical destruction of polyethylene and polypropylene. Polym Sci USSR 1967;9:2883–7. https://doi.org/10.1016/0032-3950(67)90153-0.
[85] Blumm J, Lindemann A, Meyer M, Strasser C. Characterization of PTFE using advanced thermal analysis techniques. Int J Thermophys 2010;31:1919–27. https://doi.org/10.1007/s10765-008-0512-z.
[86] Conte M, Igartua A. Study of PTFE composites tribological behavior. Wear 2012;296:568–74. https://doi.org/10.1016/J.WEAR.2012.08.015.
[87] Husain E, Nema RS. Analysis of paschen curves for air, N2 and SF6 using the townsend breakdown equation. EI-17 IEEE Trans Electr Insul1982:350–3. https://doi.org/10.1109/TEI.1982.298506.
[88] Nakayama K, Masaaki T. Simulation analysis of triboplasma generation using the particle-in-cell/Monte Carlo collision (PIC/MCC) method. J Phys D Appl Phys 2012;45:495203.
[89] Rouzic J Le, Reddyhoff T. Spatially resolved triboemission measurements. Tribol Lett 2014;55:245–52. https://doi.org/10.1007/s11249-014-0352-x.
[90] Nakayama K, Suzuki N, Hashimoto H. Triboemission of charged particles and photons from solid surfaces during frictional damage. J Phys D Appl Phys 1992;25. https://doi.org/10.1088/0022-3727/25/2/027.
[91] Dickinson JT, Scudiero L, Ã KY, Kim M, Langford SC. Dynamic tribological probes : particle emission and transient electrical measurements. Tribol Lett 1997;3:53–67. https://doi.org/10.1023/A:1019187812406.
[92] Nevshupa RA, Hiratsuka K. Fundamentals of friction and wear. Berlin; 2007. https://doi.org/10.1007/978-3-540-36807-6.
[93] Ohuchi H, Enomoto Y. Frictional heat-stimulated exo-electron emission from alumina sliding surfaces. Appl Phys Lett 1995;66:1205–7. https://doi.org/10.1063/1.113237.
[94] Dickinson JT, Donaldson EE. Autographs from peeling pressure sensitive adhesives: direct recording of fracture-induced photon emission. J Adhes 1987;24:199–220. https://doi.org/10.1080/00218468708075427.
[95] Dickinson JT, Shin JJ, Jiang W, Norton MG. Neutral and ion emissions accompanying pulsed excimer-laser irradiation of polytetrafluoroethylene. J Appl Phys 1993;74:4729–36.
[96] Evdokimov VD. Specific features of exoelectron emission during friction of metals. Sov Phys J 1972;11:11–3. https://doi.org/10.1007/BF01890910.
[97] Dickinson JT, Donaldson EE, Park MK. The emission of electrons and positive-ions from fracture of materials. J Mater Sci 1981;16:2897–908.
[98] Kim MW, Langford SC, Dickinson JT. Electron and photon emission accompanying the abrasion of MgO with diamond. Tribol Lett 1995;1:147–57.
[99] Pence S, Novotny VJ, Diaz AF. Effect of surface moisture on contact charge of polymers containing ions vol. 10. 1994.
[100] Xie L, Bao N, Jiang Y, Zhou J. Effect of humidity on contact electrification due to collision between spherical particles. AIP Adv 2016;6. https://doi.org/10.1063/1.4944831. 035117.